Journal of Power Sources 307 (2016) 796–805

Contents lists available at ScienceDirect

Journal of Power Sources

journal homepage: www.elsevier.com/locate/jpowsour

Modification of photoelectrode with thiol-functionalized Calix[4]arenes as interface energy barrier for high efficiency in dye-sensitized solar cells

Seçkin Akın [a], Mahir Gülen [a], Serkan Sayın [b], Hacer Azak [c], Hüseyin Bekir Yıldız [d], Savaş Sönmezoğlu [a, *]

[a] Department of Materials Science and Engineering, Karamanoğlu Mehmetbey University, Karaman, Turkey
[b] Department of Environmental Engineering, Giresun University, Giresun, Turkey
[c] Department of Chemistry, Karamanoğlu Mehmetbey University, Karaman, Turkey
[d] Department of Materials Science and Nanotechnology Engineering, KTO Karatay University, Konya, Turkey

HIGHLIGHTS

- A series of calix[4]arene derivatives bearing diverse group are synthesized.
- Calix[4]arenes derivatives as interfacial layer are used at photoanode in DSSCs.
- Electron-recombination and -drawbacks prevent using Calix[4]arenes derivatives.
- Efficiency of TiO_2 based DSSCs using energy barrier layers enhanced ~90%.

ARTICLE INFO

Article history:
Received 11 September 2015
Received in revised form
24 December 2015
Accepted 3 January 2016
Available online 1 February 2016

Keywords:
Dye-sensitized solar cells
Interface modification
Thiol-functionalized calixarenes
Conversion efficiency

ABSTRACT

We successfully synthesize a series of bis-thiol-substituted calix[4]arene derivatives bearing diverse groups on the upper-rim/lower-rim (**C@SH-1**, **C@SH-2**, **C@SH-3**, **C@SH-4**, **C@SH-5**). For the first time, we apply these derivatives as interface modifiers for improving the photovoltaic response of a Ru-bipy dye (N-719)-sensitized TiO_2 photoanode in dye-sensitized solar cells (DSSCs). We use FT-IR, H- and C-NMR, UV–vis spectrophotometry, and elemental analysis techniques to characterize the structures of the calix[4]arene derivatives. We achieve an overall photon-to-electron conversion efficiency (PCE) of 12.97% with the DSSCs based on 25,27-bis(5-thiol-1-oxypentane)-26,28-dihydroxycalix[4]arene (**C@SH-3**)-modified TiO_2 photoanode (J_{sc} = 9.49 mA cm^{-2}, V_{oc} = 672 mV, FF = 61.1%) compared with a system of bare TiO_2 (PCE: 6.82%) under AM 1.5G illumination of 300 W/m^2. In addition, we also study the influence of the chain length (**C@SH-2**; with 3 carbons and **C@SH-3**; with 5 carbons) and subsidiary ligand groups such as alkyl (**C@SH-1**), nitro (**C@SH-4**), and amine (**C@SH-5**) on the surface morphology, spectral response, and photovoltaic performance. Our results reveal that the C@SH-3 calixarene is the best derivative for modifiying the TiO_2 photoanode. Thiol-functionalized Calix[4]arene molecules play a role in assisting charge separation and preventing back recombination, which accounts for the observed enhancement in photovoltaic performance.

1. Introduction

Conventional dye-sensitized solar cells (DSSCs) were first invented by Michael Gratzel et al. in 1991, and countless studies have been conducted since then to further improve the performance of these devices [1,2]. Among DSSC components, the photoanode (especially TiO_2) is known to play a crucial role in achieving a high DSSC efficiency. To improve overall solar cell performance, it is essential to control and optimize the properties of the corresponding photoanode film.

A photoanode mainly suffers from relatively rapid electron–hole recombination and a large back electron transfer rate that limit the photon-to-electron conversion efficiency (PCE). The

* Corresponding author.
E-mail address: svssonmezoglu@kmu.edu.tr (S. Sönmezoğlu).

http://dx.doi.org/10.1016/j.jpowsour.2016.01.015
0378-7753/

recombination of (i) the excited electron in the LUMO level of the dye with the hole in its HOMO level, (ii) the injected electrons in the photoanode conduction band with I_3^- ions in the electrolyte, (iii) the electrons in the photoanode conduction band with holes in the HOMO level of the dye, and (iv) the electrons in the conducting glass with I_3^- ions in the electrolyte are possible unfavorable reactions that may occur in DSSCs [3,4]. Among these reactions, back electron transfer from the photoanode surface to the electrolyte is the primary reason behind the low open circuit potential (V_{oc}) and the low fill factor (FF).

Many approaches have been reported to minimize the back electron transfer rate and charge recombination [5–7]. Interface modification at the TiO_2 surface of DSSCs is one of the most effective approaches to significantly suppress charge recombination by improving the electron injection and electron transport. Interface modification of TiO_2 by other materials can produce a tunneling barrier between the photoanode and the photosensitizer that suppresses the dark current arising from the reduction of the redox electrolyte at the TiO_2 surface; this process accordingly improves the V_{oc} and FF. A modifier layer can also alter the optical properties of DSSCs by introducing an enhanced surface area on the TiO_2 layer. Given stronger dye adsorption on the modified TiO_2 surface, which results in better light absorption, J_{sc} and the efficiency can be both enhanced [8]. Therefore, it is critically important to synthesize controllable TiO_2 nanostructures with a large surface area and optimized electron transfer.

Recently, there have been some attempts to use well-known interface modifiers that modify the photoanode/dye interface that include the use of aluminum oxide (Al_2O_3) [9], zirconium dioxide (ZrO_2) [10], niobium pentoxide (Nb_2O_5) [11], and nitrogen-reduced graphene oxide (N-rGO) [12]. While oxide-based inorganic materials are widely used as modifier layers [11], there have been very few reports about the synthesis of TiO_2 using a polymer-assisted approach [13]. For instance, Sewvandi et al. used an organic silane interposed layer to modify the TiO_2 electrode interface. According to this report, the back electron transfer rate on the TiO_2 surface was drastically reduced by using {010}-faceted TiO_2 nanoparticles with six different kinds of silane. Improvements in V_{oc} and FF values have also been reported with interface modification [3]. However, the majority of known polymer-assisted materials are limited in their ability to increase the absorption of visible light, the TiO_2 surface area, and the charge transfer rate. To overcome these limitations, there have been continued attempts to develop and explore an interface modifier [14]. Here, we report several examples of thiol functionalized calix[4]arenes that can be used as an interface modifier to enhance the dye-adsorbing ability of the photoanode and suppress the recombination rate.

Calixarenes are appealing subjects for research because these molecules can be functionalized in myriad ways to yield interesting and useful materials. As a result of their ease of synthesis, worldwide demand for calix[4]arene-based devices has remarkably increased. Calixarenes derived from a condensation of phenol and formaldehyde are classified as third-generation supramolecules [15–18]. The functionalization of calixarenes with thiol moieties has been attracted significant attention due to the host-guest type ability of calixarenes and the easy binding sites provided by the thiol groups [19–21]. Moreover, thiols are able to remove contamination and oxidation from surfaces, a process that effectively cleans the surfaces for attachment [22].

Up until now, studies of thiol-functionalized calix[4]arene-modified TiO_2 photoanode-based DSSCs have not been reported. Our study can accordingly provide an experimental basis for preparing and using these designs. The goal of our work is to increase the number of thiol-substituted calix[4]arene derivatives in order to provide easily binding sites onto TiO_2 photoanodes. We have tested different types of thiol-functionalized calixarenes to enhance light-harvesting capabilities, and we use the interface-modification strategy to increase the surface area, broaden the light absorption spectra, and suppress back electron transportation. This strategy extends J_{sc} by increasing the light-harvesting ability and increases V_{oc} by minimizing the back electron transfer rate and/or charge recombination. Therefore, a feasible strategy to further improve the PCE is to develop new designs that can be used as interface modifiers at the bare TiO_2/dye interface.

2. Experimental part

2.1. Materials

We performed TLC analyses using DC Alufolien Kieselgel 60 F_{254} (Merck). Solvents were usually dried by keeping them in molecular sieves (Aldrich; 4 Å, 8–12 mesh). We carried out all of reactions under nitrogen atmosphere. We have used all of starting materials and reagents by standard analytical grade from Merck or Aldrich without additional purification. Furthermore, we prepared all of aqueous solutions with deionized water obtained using a water purification system (Millipore milli-Q Plus).

2.2. Synthesis

p-tert-Butylcalix[4]arene (**1**), 5,11,17,23-tetra-*tert*-butyl-25,27-bis-(bromopropoxy)-26,28-dihydroxycalix[4]arene (**2**), 5,11,17,23-tetra-*tert*-butyl-25,27-bis(3-thiol-1-oxypropane)-26,28-dihydroxycalix[4]arene (**3**), calix[4]arene (**4**), and 25,27-bis-(bromopropoxy)-26,28-dihydroxycalix[4]arene (**5**) were synthesized according to literature procedures [20,23–26] 25,27-bis(3-thiol-1-oxypropane)-26,28-dihydroxycalix[4]arene (**6**), 5,17-Dinitro-25,27-bis(3-bromo-1-oxypropane)-26,28-dihydroxycalix[4]arene (**7**), 5,17-Dinitro-25,27-bis(3-thiol-1-oxypropane)-26,28-dihydroxycalix[4]arene (**8**), 5,17-diamino-25,27-bis(3-bromo-1-oxypropane)-26,28-dihydroxycalix[4]arene (**9**), 5,17-diamino-25,27-bis(3-thiol-1-oxypropane)-26,28-dihydroxycalix[4]arene (**10**), 25,27-bis(5-bromo-1-oxypentane)-26,28-dihydroxycalix[4]arene (**11**), and 25,27-bis(5-thiol-1-oxypentane)-26,28-dihydroxycalix[4]arene (**12**) are herein reported for the first time.

2.2.1. Synthesis of 5,11,17,23-tetra-tert-butyl-25,27-bis(3-thiol-1-oxypropane)-26,28-dihydroxycalix[4]arene (3)

Yield: 40%; m.p.: 203–205 °C. FTIR (ATR): (see Supplementary data, Fig. S1). ^{1}H NMR (400 MHz $CDCl_3$): δ 1.19 (s, 18H, Bu^t), 1.22 (s, 18H, Bu^t), 1.57–1.69 (m, 2H, −SH), 2.42–2.48 (m, 4H, $-CH_2$-), 3.24 (t, 4H, J = 8.0 Hz, $-CH_2$-S), 3.38 (d, 4H, J = 12.8 Hz, Ar−CH_2−Ar), 4.01 (t, 4H, J = 4.8 Hz, $-CH_2$-O), 4.23 (d, 4H, J = 12.8 Hz, Ar−CH_2−Ar), 7.01 (s, 4H, ArH), 7.07 (s, 4H, ArH), 9.13 (s, 2H, −OH). Anal. Calcd. For $C_{50}H_{68}O_4S_2$: C, 75.33; H, 8.60. Found (%); C, 75.45; H, 8.79.

2.2.2. Synthesis of 25,27-bis(3-thiol-1-oxypropane)-26,28-dihydroxycalix[4]arene (6)

25,27-bis-(bromopropoxy)-26,28-dihydroxycalix[4]arene **5** (0.7 g, 1.05 mmol) was suspended in 40 mL and refluxed for 10 min. Subsequently, thiourea (0.3 g, 4.20 mmol) was added to the mixture and allow to stir under reflux for 28 h. The reaction was monitored by using a TLC (CH_2Cl_2:hexane (1:1)). The solvent was evaporated to dryness, and a solution of 0.36 g of KOH (6.41 mmol) in 40 mL of deionized water was added and allowed to reflux for further 2 h. The residue was extracted with 1 M HCl and $CHCl_3$, dried over $MgSO_4$ to afford pure compound **6** with 52% yield-m.p.: 305–306 °C. FTIR (ATR): (see Supplementary data, Fig. S2). ^{1}H NMR (400 MHz $CDCl_3$): δ 1.66 (t, 2H, J = 8.0 Hz −SH), 2.29–2.38 (m,

4H, $-CH_2$-), 3.11–3.18 (m, 4H, $-CH_2$-S), 3.41 (d, 4H, J = 12.8 Hz, Ar$-CH_2-$Ar), 4.15 (t, 4H, J = 6.0 Hz, $-CH_2$-O), 4.29 (d, 4H, J = 12.8 Hz, Ar$-CH_2-$Ar), 6.67 (t, 2H, J = 7.6 Hz, ArH), 6.76 (t, 2H, J = 7.2 Hz, ArH), 6.93 (d, 4H, J = 7.6 Hz, ArH), 7.07 (d, 4H, J = 7.6 Hz, ArH), 8.10 (s, 2H, −OH). ^{13}C NMR (100 MHz $CDCl_3$): δ 21.41, 31.44, 31.91, 74.03, 119.20, 125.59, 127.93, 128.51, 129.04, 133.29, 134.29, 151.42, 153.14. Anal. Calcd. For $C_{34}H_{36}O_4S_2$: C, 71.30; H, 6.34. Found (%); C, 71.28; H, 6.46.

2.2.3. Synthesis of 5,17-dinitro-25,27-bis(3-bromo-1-oxypropane)-26,28-dihydroxycalix[4]arene (7)

65% HNO_3 (10 mL) was added to the solution of dibromo derivative of calix[4]arene (**5**) (0.4 g, 0.6 mmol) in 20 mL of CH_2Cl_2. The mixture was stirred at room temperature for 1 h. Then, 50 mL water was poured into the mixture, and extracted. The organic phase was dried over $MgSO_4$. The residue crude was purified with hot acetone. Yield; 78.6%. Melting point; 188–190 °C. FTIR (ATR): 1333 and 1656 cm^{-1} (N–O) (see Supplementary data, Fig. S3). ^{1}H NMR (400 MHz $CDCl_3$): δ 2.59 (p, 4H, J = 6.0 Hz, $-CH_2$-), 3.56 (d, 4H, J = 13.2 Hz, Ar$-CH_2-$Ar), 3.96 (t, 4H, J = 6.4 Hz, $-CH_2$-Br), 4.21 (t, 4H, J = 5.6 Hz, O$-CH_2$-), 4.29 (d, 4H, J = 13.2 Hz, Ar$-CH_2-$Ar), 6.88 (t, 2H, J = 8.0 Hz, ArH), 7.01 (d, 4H, J = 7.6 Hz, ArH), 8.06 (s, 4H, ArH), 9.06 (s, 2H, −OH). Anal. Calcd. For $C_{34}H_{32}Br_2N_2O_8$: C, 53.99; H, 4.26; N, 3.70. Found (%); C, 54.02; H, 4.23; N, 3.64.

2.2.4. Synthesis of 5,17-dinitro-25,27-bis(3-thiol-1-oxypropane)-26,28-dihydroxycalix[4]arene (8)

A mixture of **7** (0.1 g, 0.144 mmol) and thiourea (0.04 g, 0.574 mmol) in CH_3CN (20 mL) was refluxed for 17 h. The volatile components were evaporated, and a solution of 0.5 g of KOH in 4 mL of deionized water was added and allowed to reflux for further 2 h. Then, 1 M HCl was slowly added and filtered, and washed with water to adjust pH 7.0. The crude was purified by column chromatography. Yield; 59.6%, m.p > 400 °C. FTIR (ATR): 1333 and 1655 cm^{-1} (N–O) (see Supplementary data, Fig. S4). ^{1}H NMR (400 MHz DMSO): δ 1.23 (s, 2H, −SH), 2.35–2.38 (m, 4H, $-CH_2$-), 3.80 (d, 4H, J = 12.8 Hz, Ar$-CH_2-$Ar), 4.07 (t, 4H, J = 6.4 Hz, $-CH_2$-), 4.13 (t, 4H, J = 6.0 Hz, $-CH_2$-), 4.23 (d, 4H, J = 12.8 Hz, Ar$-CH_2-$Ar), 6.89 (t, 2H, J = 8.0 Hz, ArH), 7.19 (d, 4H, J = 7.6 Hz, ArH), 8.30 (s, 4H, ArH), 9.43 (s, 1H, −OH). ^{13}C NMR (100 MHz DMSO): δ 29.49 (S$-CH_2$), 30.20 (Ar-CH_2-Ar), 31.55 ($-CH_2$), 74.42 (O$-CH_2$), 125.10 (Ar–*C*), 126.58 (Ar–*C*), 129.06 (Ar–*C*), 130.22 (Ar–*C*), 132.80 (Ar–*C*), 139.98 (N-Ar-*C*), 151.55 (ArO-*C*), 159.51 (ArO-*C*). Anal. Calcd. For $C_{34}H_{38}N_2O_4S_2$: C, 67.74; H, 6.35; N, 4.65. Found (%); C, 67.7; H, 6.28; N, 4.71.

2.2.5. Synthesis of 5,17-diamino-25,27-bis(3-bromo-1-oxypropane)-26,28-dihydroxycalix[4]arene (9)

Raney-Ni (1 g) was added to a mixture of the dinitro compound **7** (0.2 g, 0.264 mmol) and hydrazine (1.3 mL) in MeOH (50 mL), and the suspension was stirred at rt. After 10 h, the mixture was filtered off and the solvent was removed under reduced pressure. The residue was precipitated by addition of chloroform/hexane (10 mL/15 mL) to give the pure diamine with 83.3% yield. Melting point >400 °C. FTIR (ATR): (see Supplementary data, Fig. S5). ^{1}H NMR (400 MHz DMSO): δ 2.23–2.26 (m, 4H, $-CH_2$-), 3.60–3.62 (m, 4H, $-CH_2$-), 3.72 (d, 4H, J = 12.8 Hz, Ar$-CH_2-$Ar), 4.11 (s, 4H, $-NH_2$), 4.18 (d, 4H, J = 12.8 Hz, Ar$-CH_2-$Ar), 4.25 (t, 4H, J = 5.2 Hz, $-CH_2$-O), 6.89 (t, 2H, J = 7.6 Hz, ArH), 7.16 (d, 4H, J = 7.6 Hz, ArH), 7.25 (s, 4H, ArH), 8.05 (s, 2H, −OH). Anal. Calcd. For $C_{34}H_{36}Br_2N_2O_4$: C, 58.63; H, 5.21; N, 4.02. Found (%); C, 58.59; H, 5.33; N, 3.96.

2.2.6. Synthesis of 5,17-diamino-25,27-bis(3-thiol-1-oxypropane)-26,28-dihydroxycalix[4]arene (10)

A mixture of 5,17-diamino-25,27-bis(3-bromo-1-oxypropane)-26,28-dihydroxycalix[4]arene (**9**) (0.1 g, 0.144 mmol) and thiourea (0.04 g, 0.574 mmol) in CH_3CN (20 mL) was refluxed for 17 h. The volatile components were evaporated, and a solution of 0.5 g of KOH in 4 mL of deionized water was added and allowed to reflux for further 2 h. Then, 1 M HCl was slowly added and filtered, and washed with water to adjust pH 7.0. The crude was re-crystallized from acetone. Yield; 59.6%. Melting point >400 °C. FTIR (ATR(see Supplementary data, Fig. S6). ^{1}H NMR (400 MHz DMSO): δ 1.22 (s, 2H, −SH), 2.35–2.44 (m, 4H, $-CH_2$-), 3.31–3.55 (m, 4H, $-NH_2$ *over shielded by the solvent*), 3.61–3.67 (m, 4H, $-CH_2$-), 3.82 (d, 4H, J = 12.8 Hz, Ar$-CH_2-$Ar), 4.15 (d, 4H, J = 12.8 Hz, Ar$-CH_2-$Ar), 4.22–4.24 (m, 4H, $-CH_2$-), 6.57 (t, 2H, J = 7.6 Hz, ArH), 7.11 (d, 4H, J = 7.6 Hz, ArH), 7.93 (s, 4H, ArH), 8.29 (s, 2H, −OH). ^{13}C NMR (100 MHz DMSO): δ 26.99 (S$-CH_2$), 30.65 ($-CH_2$), 31.85 (Ar-CH_2-Ar), 73.36 (O$-CH_2$), 120.12 (Ar–*C*), 124.39 (Ar–*C*), 128.21 (Ar–*C*), 129.79 (Ar–*C*), 131.44 (Ar–*C*), 137.43 (N-Ar-*C*), 153.11 (ArO-*C*), 164.70 (ArO-*C*). Anal. Calcd. For $C_{34}H_{38}N_2O_4S_2$: C, 67.74; H, 6.35; N, 4.65. Found (%); C, 67.7; H, 6.28; N, 4.71.

2.2.7. Synthesis of 25,27-bis(5-bromo-1-oxypentane)-26,28-dihydroxycalix[4]arene (11)

A mixture of calix[4]arene (3.0 g, 7.0 mmol), K_2CO_3 (1.9 g, 14.0 mmol) and the dibromopropane (9.7 g, 42.14 mmol) in dry CH_3CN (150 mL) was stirred for 28 h. The solvent was then evaporated under vacuum and the residue taken up with $CHCl_3$. The organic phase was washed with 0.1 M HCl up to neutrality and dried over anhydrous $MgSO_4$. The resulting crude product was purified by addition of MeOH. Yield; 29%. ^{1}H NMR (400 MHz $CDCl_3$): δ 1.86–1.93 (m, 8H, $-CH_2$-), 2.06–2.12 (m, 4H, $-CH_2$-), 3.42 (d, 4H, J = 13.2 Hz, Ar$-CH_2-$Ar), 3.52 (t, 4H, J = 6.8 Hz, $-CH_2$-Br), 4.02 (t, 4H, J = 6.8 Hz, $-CH_2$-O), 4.29 (d, 4H, J = 13.2 Hz, Ar$-CH_2-$Ar), 6.67 (t, 2H, J = 7.6 Hz, ArH), 6.74 (t, 2H, J = 7.6 Hz, ArH), 6.91 (d, 4H, J = 7.6 Hz, ArH), 7.07 (d, 4H, J = 7.6 Hz, ArH), 8.06 (s, 2H, −OH). Anal. Calcd. For $C_{38}H_{42}Br_2O_4$: C, 63.17; H, 5.86. Found (%); C, 63.03; H, 5.72.

2.2.8. Synthesis of 25,27-bis(5-thiol-1-oxypentane)-26,28-dihydroxycalix[4]arene (12)

A mixture of 25,27-bis(5-bromo-1-oxypentane)-26,28-dihydroxycalix[4]arene (**11**) (1.07 g, 1.48 mmol) and thiourea (0.37 g, 4.97 mmol) in 40 mL of CH_3CN was refluxed for 30 h. The reaction was monitored by using a TLC (CH_2Cl_2:hexane (1:1)). The solvent was evaporated to dryness, and a solution of 0.51 g of KOH (6.41 mmol) in 21 mL of deionized water was added and allowed to reflux for further 2 h. The residue was extracted with 1 M HCl and $CHCl_3$, dried over $MgSO_4$ to produce viscose **12** with 52% yield. FTIR (ATR): (see Supplementary data, Fig. S7). ^{1}H NMR (400 MHz $CDCl_3$): δ 1.51 (brs, 2H, −SH), 1.87 (brs, 8H, $-CH_2$-), 2.12 (brs, 4H, $-CH_2$-), 2.68 (brs, 4H, $-CH_2$-S), 3.44 (d, 4H, J = 12.8 Hz, Ar$-CH_2-$Ar), 4.06 (brs, 4H, $-CH_2$-O), 4.35 (d, 4H, J = 12.8 Hz, Ar$-CH_2-$Ar), 6.72–6.77 (m, 4H, ArH), 6.95 (d, 4H, J = 7.6 Hz, ArH), 7.11 (brs, 4H, ArH), 8.21 (s, 2H, −OH). Anal. Calcd. For $C_{38}H_{44}O_4S_2$: C, 72.57; H, 7.05. Found (%); C, 72.48; H, 6.96.

2.3. Fabrication of DSSCs

We manufactured TiO_2 nanoparticle-based films; the details of this process appear in our previous work [27]. We then used thiol-substituted calix[4]arene derivatives (**C@SH-1**, **C@SH-2**, **C@SH-3**, **C@SH-4** and **C@SH-5**) obtained as interface modifiers for TiO_2 nanoparticle-based films. The interface modifier solution of all thiol-substituted calix[4]arene derivatives was prepared in a dichloromethane (DCM, or methylene chloride) solvent under exactly the same conditions. We carried out interface modification of the TiO_2 films using a well-known approach: the spin-coating

process. We performed the spinning process using a Holmarc Spin Coating Unit, and we completed the overcoating by rapidly depositing ~30 μL of solution onto a TiO_2 paste-coated FTO (Fluorine doped Tin Oxide) glass substrate spun at 3000 rpm for 30 s in air. We repeated this process five times on each substrate to obtain a homogeneous surface. To fabricate the working electrodes (photoanodes), we immersed the modified films in a dye solution (a mixture of ruthenizer 535-bisTBA (N-719) in methanol) for 12 h. The I^-/I_3^- electrolytes and Pt counter electrodes were prepared according to our previous report [28]. We fabricated the device according to the following method: The photoanode was placed face up on a flat surface, and the catalyst-coated counter electrode was placed on top of the photoanode. These two opposing glass plates were offset from one another so that the entire photoanode was covered by the counter electrode. The I^-/I_3^- electrolyte solution was placed at the edges of the plates, and the liquid was drawn into the space between the electrodes via capillary action. We used an epoxy adhesive to hold the electrodes together. We accordingly fabricated both calix[4]arene-modified and bare TiO_2 (as a reference device) photoanode-based DSSCs. A schematic structure of the thiol-functionalized, calixarene-modified, TiO_2 photoanode-based DSSC is shown in Fig. 1. We defined the active working area as 0.8 cm^2.

2.4. Characterizations

We determined the melting points of thiol-substituted calix[4]arene derivatives on a Gallenkamp apparatus in a sealed capillary glass tube. We recorded proton nuclear magnetic resonance (^1H NMR) spectra on a Varian 400 MHz spectrometer. We performed elemental analyses using a Leco CHNS-932 analyzer. Fourier transform infrared spectroscopy (FTIR) spectra were recorded on a Perkin Elmer 1605 FTIR System Spectrometer. We conducted ultraviolet (UV)-visible absorption measurements of the calix[4]arene-modified and bare photoanodes using a dual wavelength/double beam Shimadzu UV-3600 spectrophotometer. We analyzed the morphology of the photoanodes using a JEOL 6390-LV Scanning Electron Microscope (SEM) with an accelerating voltage of 20 kV in the secondary electron image mode. We carried out cyclic voltammetry (CV) studies and electrochemical impedance spectroscopy (EIS) using an Ivium-compactStat model potentiostat/galvanostat in a three-electrode configuration. The current–voltage (I–V) curves were recorded using a Keithley 4200 SCS characterization system. The light source was a 300 W xenon arc lamp with a filter to simulate the AM 1.5 Solar Light XPS 300 solar spectrum. We measured the wavelength-dependent incident photon-to-charge carrier efficiency (IPCE) using an Enlitech QE-R system with a 75 W xenon arc lamp source.

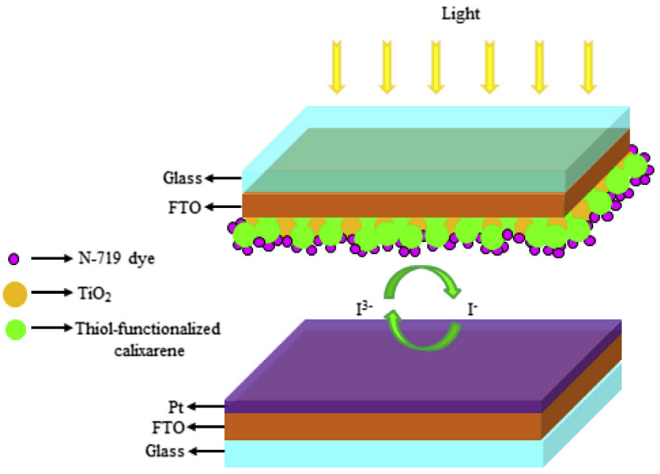

Fig. 1. The representative structure of calix[4]arene modified TiO_2 photoanode based DSSC.

3. Results & discussion

3.1. Tailored upper-rim functionalization of novel bis-thiol-substituted calix[4]arene derivatives

The goal of the synthetic part of this study was to synthesize bis-thiol-substituted calix[4]arene derivatives, which were selectively functionalized with different groups on the upper rim of calix[4]arenes. For this purpose, we synthesized *p-tert*-Butylcalix[4]arene (**1**), 5,11,17,23-tetra-*tert*-butyl-25,27-bis(bromo propoxy)-26,28-dihydroxycalix[4]arene (**2**) and 5,11,17,23-tetra-*tert*-butyl-25,27-bis(3-thiol-1-oxypropane)-26,28-dihydroxycalix [4]arene (**3**) according to procedures noted in the literature [20,23,24] (see Scheme 1).

Calix[4]arene (**4**), consisting of the de-alkylation of *p-tert*-butylcalix[4]arene (**1**) in the presence of phenol and $AlCl_3$, was treated with 1,3-dibromopropane or 1,5-dibromopropane in CH_3CN to yield 25,27-bis-(bromopropoxy)-26,28-dihydroxycalix[4]arene (**5**) (synthesis of **5** has been reported elsewhere [25,26]) or 25,27-bis(5-bromo-1-oxypentane)-26,28-dihydroxycalix[4]arene (**11**). We accordingly obtained dibromine derivatives of calix[4]arene **5** or **11,** and we converted these derivatives to their corresponding derivatives 25,27-bis(3-thiol-1-oxypropane)-26,28-dihydroxycalix [4]arene (**6**) and 25,27-bis(5-thiol-1-oxypentane)-26,28-dihydroxycalix[4]arene (**12**) via a reaction with thiourea in CH_3CN followed by a reaction with an aqueous KOH solution to produce the cone conformer with yields of 52% and 55%, respectively (see Scheme 2).

We conducted the substitution of 25,27-bis-(bromopropoxy)-26,28-dihydroxycalix[4]arene (**5**) at its upper rim in the presence of DCM with 65% HNO_3 to produce the cone conformer 5,17-dinitro-25,27-bis(3-bromo-1-oxypropane)-26,28-dihydroxycalix[4]arene (**7**) with a yield of 79%. Upon reduction of the nitro groups with Raney-Ni, we synthesized 5,17-diamino-25,27-bis(3-bromo-1-oxypropane)-26,28-dihydroxycalix[4]arene (**9**) with a yield of 83%. To obtain thiol derivatives of both upper-rim functionalized calixarenes, we treated **7** and **9** with thiourea in acetonitril followed with an aqueous solution of KOH to yield the corresponding 5,17-dinitro-25,27-bis(3-thiol-1-oxypropane)-26,28-dihydroxycalix[4] arene (**8**) and 5,17-diamino-25,27-bis(3-thiol-1-oxypropane)-26,28-dihydroxycalix[4]arene (**10**), respectively (see Scheme 3). The structures of all calix[4]arene derivatives were confirmed using FTIR, ^1H-NMR, ^{13}C-NMR and elemental analysis techniques (see the Supplementary data, Figs. S1–S18).

To determine the structures of **C@SH-1**, **C@SH-2**, **C@SH-3**, **C@SH-4** and **C@SH-5**, we performed FT-IR (see the Supplementary data, Figs. S1–S7). Notable characteristic peaks appeared at 1333 and 1655 cm^{-1} due to the stretch vibration bands of the N–O group of **C@SH-4**; these vibration bands were clearly absent for **C@SH-5** after the reduction of the nitro groups of the corresponding dibromine derivative **7**.

The ^1H NMR spectra indicate that all thiol-substituted calix[4]arene derivatives state in cone conformer due to the having characteristic two doublet peaks of methylene bridge proton ($ArCH_2Ar$) at approximately 3.35 and 4.29 ppm [29] (see the Supplementary data, Figs. S8–S18). One can also observe the regioselective formation of distally substituted derivative **7** with nitro groups in the ^1H NMR spectrum. However, compound **7** possesses one singlet of nitro-substituted phenyl rings with four

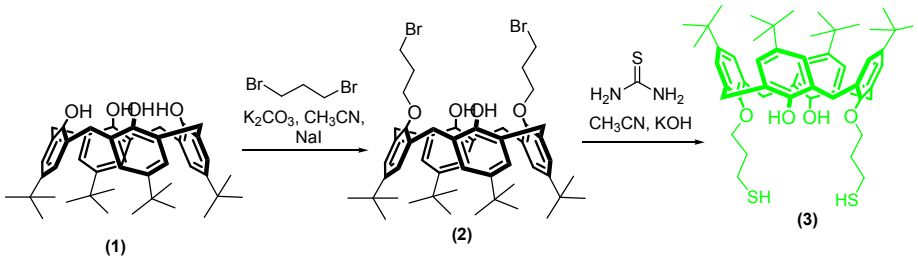

Scheme 1. Preparation of 5,11,17,23-tetra-*tert*-butyl-25,27-bis(3-thiol-1-oxypropane)-26,28-dihydroxycalix[4]arene (**C@SH-1**).

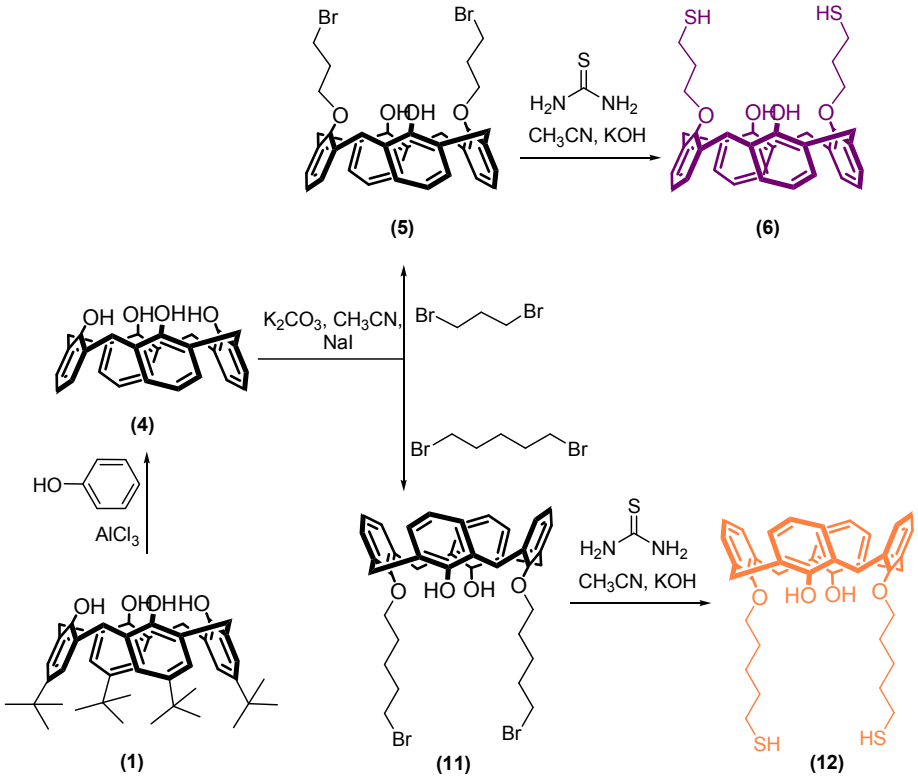

Scheme 2. Preparation of 25,27-bis(3-thiol-1-oxypropane)-26,28-dihydroxycalix[4]arene (**C@SH-2**) and 25,27-bis(5-thiol-1-oxypentane)-26,28-dihydroxycalix[4]arene (**C@SH-3**).

protons at 8.06 ppm, one doublet with four protons at 7.01 ppm and a triplet with two protons from the other phenyl rings at 6.88 ppm. The reduction process of the nitro groups (Ar-NO_2) of **7**, which converted to the Ar−NH_2 groups of the corresponding **9**, has one singlet peak with four protons at 4.11 ppm via a reduction reaction; the ^{1}H-NMR technique yields useful information. Moreover, the appearance of the additional peak, which corresponds to the protons of the −SH group at approximately δ 1.3 ppm (2H) in the ^{1}H NMR spectrum, confirm the structures of all thiol-substituted calix[4]arene derivatives (**C@SH-1**, **C@SH-2**, **C@SH-3**, **C@SH-4**, and **C@SH-5**). In addition, the peak belonging to the S−CH_2 groups appears at approximately 25 ppm in ^{13}C NMR spectra of all thiol-substituted calix[4]arene derivatives.

3.2. Photovoltaic performance of DSSCs

In order to improve the evidence of the light-absorbing effect, we attempted to measure the absorbing ability of the photoanodes so that we could understand how much light in the film was actually being absorbed by the photoanodes. The absorbance spectra of the bare and calix[4]arene-modified TiO_2 films are shown in Fig. 2. After TiO_2 film was modified by calix[4]arene, an enhancement in the absorption spectra in the visible region could be readily observed. We furthermore observed a shift in the absorption threshold toward the center of the visible-light regime for the modified TiO_2 samples.

All of these results confirm that the calix[4]arene can effectively improve the visible-light absorption properties of bare TiO_2. This result indicates that the calix[4]arene can be used to endow TiO_2 with visible-light sensitivity. Similar results have been reported for modified-TiO_2 photoanode-based DSSCs for various interface modifiers [30,31]. As clearly seen in Fig. 2, the **C@SH-3** photoanode possesses the highest absorption ability, which suggesting an increase in J_{sc}. The absorption spectra of calix[4]arene-modified photoanodes were redshifted compared with the spectra of the bare TiO_2 photoanode, an effect that is desirable for harvesting energy from the solar spectrum [32].

The rapid electron transfer kinetics of TiO_2 are necessary to avoid photoelectron recombination, which strongly depends on the

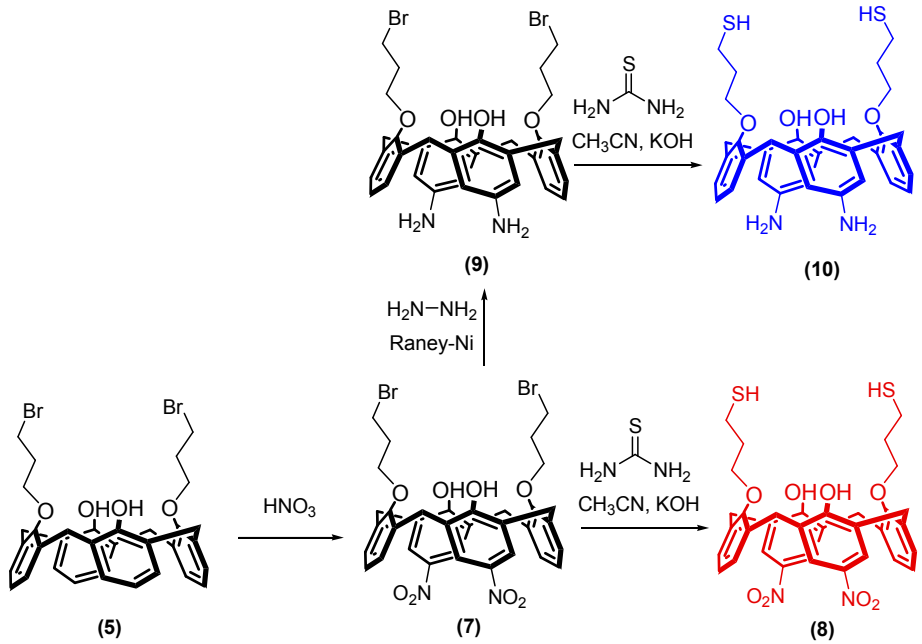

Scheme 3. Preparation of 5,17-dinitro-25,27-bis(3-thiol-1-oxypropane)-26,28-dihydroxycalix[4]arene (**C@SH-4**) and 5,17-diamino-25,27-bis(3-thiol-1-oxypropane)-26,28-dihydroxycalix[4]arene (**C@SH-5**).

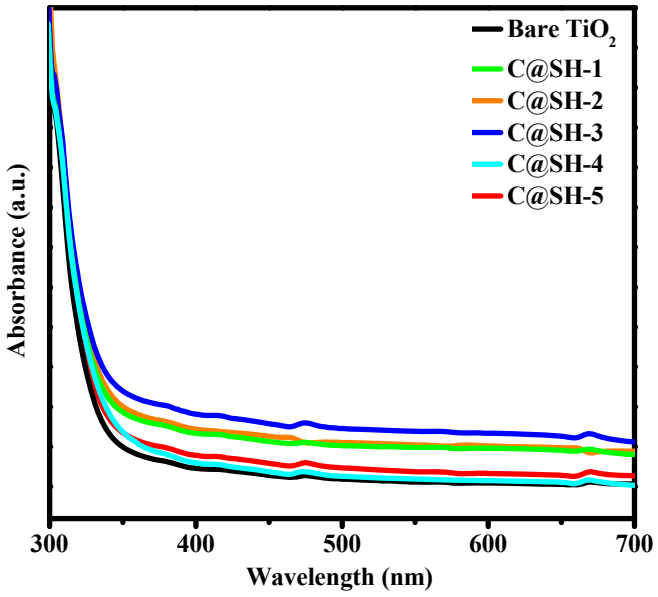

Fig. 2. Absorption spectra of bare and calix[4]arene modified TiO_2 based photoanodes.

morphology and crystallographic structure of TiO_2. For instance, an unfavorable morphology and/or poor crystallinity will typically result in more defects in the structure and therefore an increase in the recombination rate. SEM images are useful for allowing us to draw conclusions whether the overcoating of calix[4]arenes has a strong effect on the TiO_2 nanoparticle's morphology. Fig. 3 shows SEM micrographs of TiO_2 photoanodes with and without the calix[4]arene interface modifier. The TiO_2 nanoparticles modified by various calix[4]arene agents can evenly distribute on the FTO substrate with a smaller particle size; the bare TiO_2 nanoparticles exhibit obvious agglomeration due to their having a higher surface energy.

Our SEM analysis revealed that both the bare and modified films possess a crack-free and uniform structure. The bare TiO_2 film has a typical porous structure with an average particle size of 30–50 nm. In sharp contrast with the bare TiO_2 film, the calix[4]arene-modified films have surfaces that are very roughness and porous; these films also possess a compact internal structure with an average particle size of 20–30 nm. It is noteworthy that interface modification of TiO_2 nanoparticles/dye minimizes nanoparticle aggregation (on dispersion). Therefore, the porosity of these films allows electrolytes to fill in the pores of the film and make good contact with the dye molecules and electrolyte. In other words, dyes can be sufficiently adsorbed, and electrons can be quickly and efficiently transferred at the film/dye/electrolyte interfaces [33].

It is well known that porous nanocrystalline TiO_2 with a large surface area is beneficial for dye loading and improving the performance of DSSCs [34]. Moreover, previous studies have shown that some of the key parameters known to boost the efficiency of DSSCs are the surface properties of the active layer [8,35]. These SEM figures also show that the porosity of the resulting porous films can be controlled by changing the molecular design of calix[4]arenes on the TiO_2 paste.

To investigate the feasibility of electron transfer from the excited dye molecule to the conduction band of the TiO_2 electrode, we investigated the preventive potentials of the modifier layer using cyclic voltammetry (CV) with a 0.01 V s^{-1} scan rate (see the Supplementary data, Fig. S19). The energy-level alignments of the cyclic voltammograms are shown in Fig. 4. One can see that the LUMO values of these interface modifiers vary from −3.06 eV to −3.26 eV. This range is lower (more negative) than the LUMO level of the dye and higher (more positive) than the LUMO level of TiO_2. These results clearly demonstrate that a thin layer of calix[4]arene modifiers can be potentially efficient at suppressing recombination and minimizing back electron transportation in DSSC applications. The calix[4]arene barrier can prevent the recombination of the injected electron on the conduction band of TiO_2 with the dye cation. Furthermore, as a result of the calix[4]arene barrier, conduction-band electrons in TiO_2 are unable to recombine with I_3^- ions at

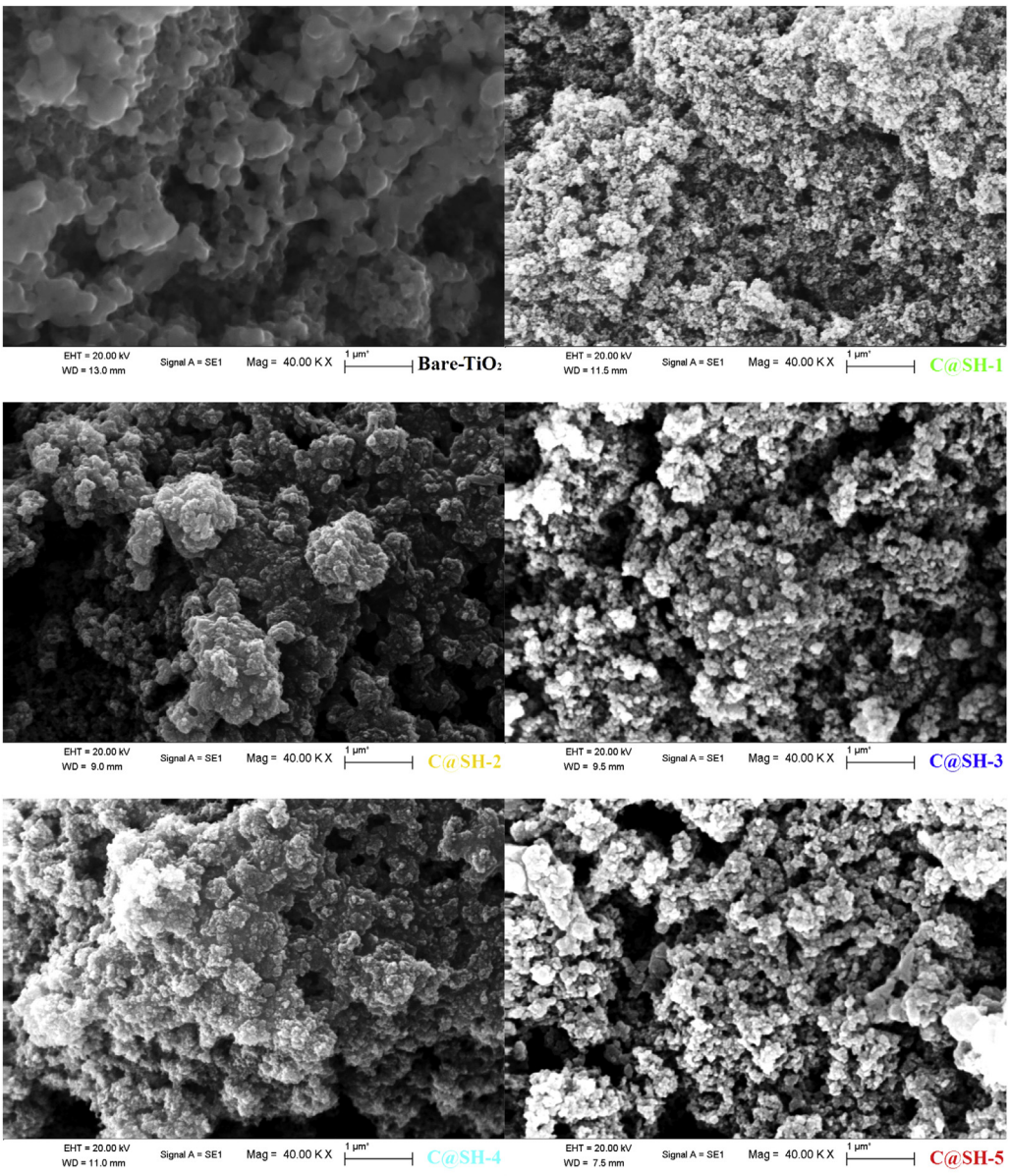

Fig. 3. SEM images (at 40 k ×) of the surface morphology of bare and, calix[4]arene derivatives modified TiO_2 paste photoanodes.

the electrolytic interface.

Current density-voltage (J-V) curves of the DSSCs with and without the modified layer are shown in Fig. 5a; we summarize the photovoltaic characteristics of these DSSCs in Table 1. Compared with traditional bare DSSCs, the performance of the DSSCs with the overlayer significantly improved using J_{sc} and V_{oc} as metrics (Fig. 5b). The **C@SH-3** cell reaches its highest PCE of 12.97% compared with 6.82% achieved by the bare TiO_2 cell under the same conditions. On the other hand, we obtain the maximum photocurrent for the **C@SH-1**-modified photoanode-based DSSC. This highest photocurrent of the **C@SH-1** cell corresponding to its high cell efficiency is 10.53 mA/cm^2, which is 34% higher than the photocurrent of its bare TiO_2 counterpart (6.92 mA/cm^2). The higher photocurrent injection of **C@SH-1** compared with bare TiO_2 can accordingly be attributed to a large extent to the much larger specific surface area and surface roughness of **C@SH-1** compared with bare TiO_2; this higher injection rate leads to a correspondingly higher dye adsorption ability based on our optical absorption spectra analyses. However, the V_{oc} of **C@SH-1** cell exhibits the lowest value of other calix[4]arene-modified, TiO_2 photoanode-based devices. This result can also be explained by the highest peak in the CV graph that suggests the lowest energy level (see the Supplementary data, Fig. S19).

The largest enhancement (~90%) in DSSC conversion efficiency (compared with that of bare TiO_2) was achieved using **C@SH-3**-assisted TiO_2 nanocrystals as photoanodes. Furthermore, the efficiency of the solar cell using longer thiol chains was markedly higher than that of both bare TiO_2 and other thiol-based, dual-ligand groups such as amine (**C@SH-5**), alkyl (**C@SH-1**) and nitro (**C@SH-4**). This finding can be explained by the long diffusion length and stronger interactions between the longer thiol chains and TiO_2, which lead increased charge transfer. We explain our results as follows: The outer layer of calix[4]arene derivatives on larger TiO_2 nanoparticles strongly adsorbs the Ru-based N-719 dye, and the photoexcited sensitizer molecules inject energetic electrons to TiO_2 tunnelling across the calix[4]arene barrier. Once the

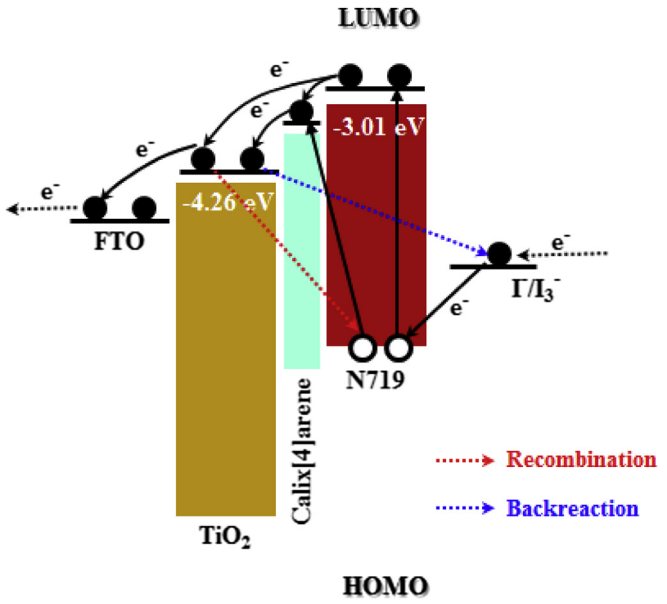

Fig. 4. Energy level diagram and mechanism of photocurrent generation in DSSCs. Schematic diagram showing the calculated positions of HOMO and LUMO levels of calix[4]arenes, with respect to the vacuum level.

electrons relax to the conduction band of TiO_2, the calix[4]arene barrier prevents the recombination of the electron with the dye cation. Furthermore, because of the calix[4]arene barrier, the conduction-band electrons in TiO_2 are unable to recombine with the I_3^- ions at the electrolytic interface. Therefore, a thin layer of calix[4]arene on TiO_2 particles suppresses both types of recombinations. Moreover, a photoanode with a high efficiency should possess a large surface area, rapid electron transport, an efficient light-harvesting ability, and low rates of electron recombination [36].

The IPCE spectra of **C@SH-1**, **C@SH-2**, **C@SH-3**, **C@SH-4**, **C@SH-5**, and bare TiO_2 photoanode-based devices are representatively depicted in Fig. 6. We measured the IPCE as a function of wavelength to evaluate the photo-response of the photoanodes over the spectral regime. As shown in Fig. 6, **C@SH-2**, **C@SH-4**, **C@SH-5**, and bare TiO_2 photoanode-based devices exhibited a broad IPCE between 400 and 600 nm, but their peak values were limited to approximately 10–15%. The substantial increase in J_{sc} of the **C@SH-1** DSSC was in good agreement with its larger IPCE in the visible regime; the larger IPCEs can be ascribed to the increased light-harvesting and charge collection efficiencies of the **C@SH-1** DSSC at these wavelengths [37,38]. On the other hand, the IPCE of the **C@SH-3** DSSC exceeded 25% over the spectral range 450–550 nm and attained its maximum of 33% with a shoulder centered at approximately 345 nm.

We carried out EIS of the calix[4]arene-modified, TiO_2 photoanode-based DSSCs to correlate the device structure with an equivalent circuit model (shown in the inset of Fig. 7) to better understand electrochemical kinetics and photo-electrochemical processes. The EIS results were recorded over the frequency range 10^{-2}–10^5 Hz with 0.75 V forward bias and 10 mV amplitude (ac) in dark media. As shown in Fig. 7, the high-frequency intercept on the real axis represents the equivalent series resistance (R_s), the first semicircle denotes the charge transport resistance (R_t) at the platinum counter electrode/electrolyte interface, and the second semicircle represents the charge transfer resistance (R_{ct}) related to electron recombination/transport between the TiO_2/dye and electrolyte interface. The EIS parameters, including R_s, R_t, R_{ct}, Q_1, α_1 associated with Q_1, Q_2 and α_2 associated with Q_2, were extracted by fitting the recorded EIS data using an equivalent circuit; these parameters are listed in Table 2. A phase-constant element (CPE) involves both the capacitance double layer (C_{dl}) and layer in the equivalent circuit model. The CPE can be defined by Eq. (1) [39] as:

$$Z(CPE) = Q^{-1}(jw)^{-\alpha} \quad (1)$$

where Z is the impedance of the CPE, Q is the CPE constant, w is the angular frequency, j = 1 is the imaginary unit and α is the power of the CPE related to the phase shift. When the power of the CPE is equal to 1, 0 or −1, the CPE can be defined as a classical lumped model capacitor (C), resistance (R) or inductance (L), respectively. Furthermore, the value of n = 0.5 denotes the Warburg impedance (W). In case of low α values, the surface roughness and

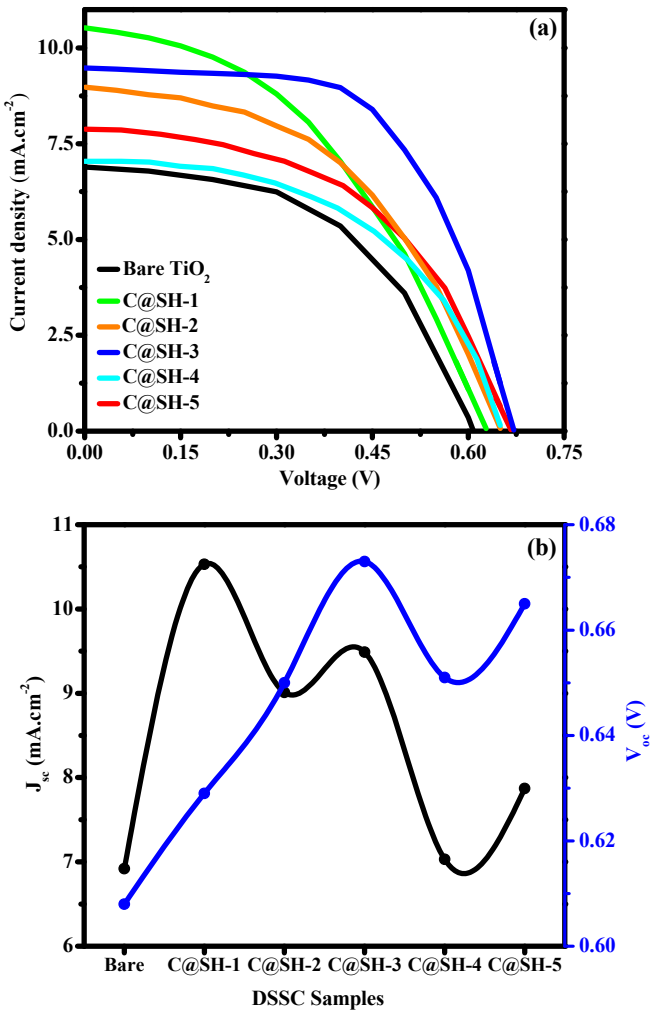

Fig. 5. (a)- The J-V curves of bare and calix[4]arene modified TiO_2 photoanode based DSSC devices **(b)-** The obtained J_{sc} and V_{oc} values as a function of photoanodes.

Table 1
Summary of the photovoltaic characteristics of DSSCs.

Samples	V_{oc} (mV)	J_{sc} (mA cm^{-2})	FF (%)	PCE
C@SH-1	629	10.53	45.2	9.98
C@SH-2	650	9.01	49.2	9.60
C@SH-3	672	9.49	61.1	12.97
C@SH-4	651	7.03	52.6	8.02
C@SH-5	665	7.87	51.5	8.98
Bare TiO_2	608	6.92	48.6	6.82

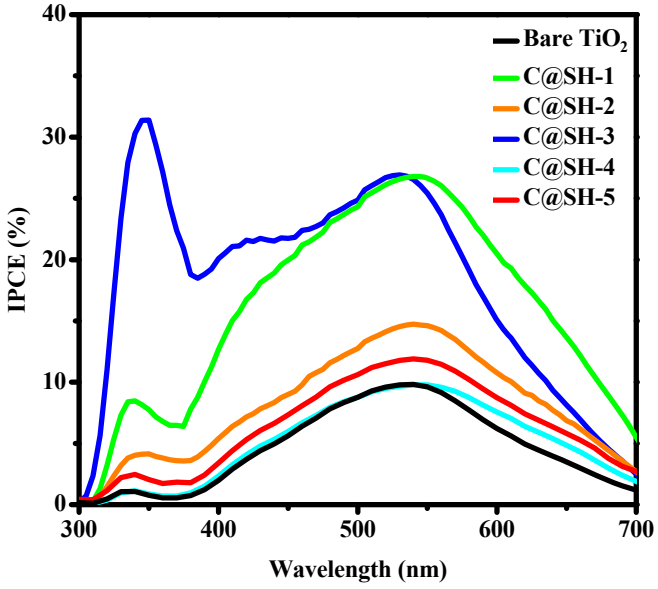

Fig. 6. IPCE spectra of bare and calix[4]arene modified TiO_2 photoanode based DSSC devices.

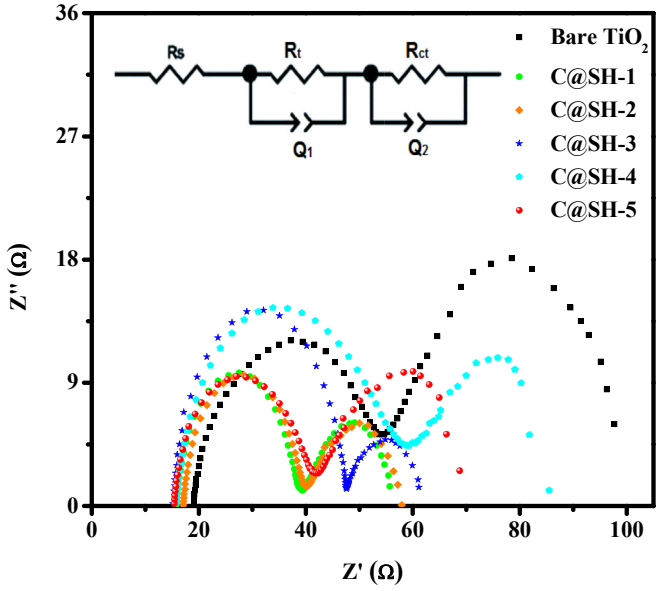

Fig. 7. Nyquist plot of bare and calix[4]arene modified TiO_2 photoanode based DSSC devices.

$$C_{dl} = \left(Q.R^{1-\alpha}\right)^{1/\alpha} \quad (2)$$

From Table 2, one can see that the values of R_s decrease with calix[4]arene modification compared with the bare TiO_2 film. This trend indicates that the interfacial resistance between the FTO substrate and the TiO_2 film is reduced in the presence of modified calix[4]arene on the TiO_2 film. Besides Rs, the R_{ct} parameter, which is responsible for electron recombination and transfer, varied from 14.00 to 45.34 Ω. R_{ct} was significantly reduced after calix[4]arene modification as the interface energy barrier, which may be due to the increased acceleration of the electron transfer process in the calix[4]arene-TiO_2 photoanode and led to better cell performance. The lowest R_{ct} value confirms that the C@SH-3 photoanode-based DSSC of all the calix[4]arene derivates was the best interface energy barrier for retarding the electron backward transport and therefore resulted in a higher DSSC PCE. Furthermore, we calculated the electron life time (τ_n) of the DSSCs using the equation $\tau_n = C_{dl2} \cdot R_{ct}$, where R_{ct} and C_{dl2} are the charge transfer resistance and the capacitance at the TiO_2/calix[4]arene/dye structure and electrolyte interface, respectively. The double-layer capacitance is an equilibrium property that relates variations in the carrier density to the displacement of the Fermi level [42]. As shown in Table 2, the estimated electron lifetime value for C@SH-3 modified TiO_2-based DSSC is the longest value; the estimated electron lifetime for bare TiO_2 is the shortest value. It is known that a larger electron lifetime value leads to a decrease in the recombination rate of injected electrons and enhances the electron transport rate, which leads to an improved J_{sc} value. This can be attributed to longer thiol chains and thiol-based, dual-ligand groups such as amine, alkly and nitro in calixarene derivatives. Moreover, an increase in the electron lifetime results in a larger electron diffusion length (L) and diffusion coefficient (D). Therefore, we can conclude that the charge transfer process is improved by modifying TiO_2 with calix[4]arene derivatives.

4. Conclusions

A new series of thiol-functionalized calix[4]arene derivatives that bear different substituents was selectively synthesized. These thiol-functionalized calix[4]arene derivatives were successfully immobilized onto TiO_2 paste films in order to enhance light-harvesting capabilities, and to suppress the back reaction mechanisms. From the viewpoint of the characterization of the DSSC devices, the following results have been determined: i-) The absorbance results show interface modified TiO_2 photoanodes extend the absorption edge to the visible light range and make the red shift more distinct. ii-) Higher surface area TiO_2 with a porous structure by overcoating of calix[4]arene derivatives which imply a greater real surface extension has been observed in SEM micrographs. iii-) ~90% enhancement in the cell efficiency of **C@SH-3** compared to the bare TiO_2 based DSSC and a high fill factor beyond

Table 2
The EIS results obtained from fitting the equivalent circuit model and the estimated electrochemical kinetics of fabricated DSSCs.

Samples	R_s (Ω)	R_t (Ω)	R_{ct} (Ω)	$Q_1 \times 10^{-5}$ ($Fs\alpha^{-1}$)	α_1	$Q_2 \times 10^{-3}$ ($Fs\alpha^{-1}$)	α_2	C_{dl2} (mF)	τ_n (s)
C@SH-1	15.64	23.62	18.43	2.47	0.874	51.57	0.789	50.87	0.94
C@SH-2	16.12	22.80	17.49	2.33	0.886	52.01	0.749	50.39	0.88
C@SH-3	15.99	32.53	14.00	1.45	0.920	81.79	0.829	84.10	1.18
C@SH-4	15.68	44.69	28.74	7.63	0.734	27.85	0.821	26.53	0.76
C@SH-5	15.91	26.66	32.22	5.05	0.793	26.52	0.703	24.82	0.80
Bare TiO_2	17.05	37.44	45.34	13.70	0.714	16.21	0.819	15.14	0.69

heterogeneity of the photoanode are high [40]. To investigate the electron lifetime (τ_n), the C_{dl} values can be derived from the CPE parameters using Eq. (2) [41]:

61.1%, owing to the higher dye adsorption, and faster photon/electron transportation of the photoanode due to the profound impact of thiol chain length. iv-) As a ligand group addition to thiol, alkyl based DSSC (**C@SH-1**) shows more efficiency than nitro (**C@SH-4**) and amine (**C@SH-5**) based ones. v) The thiol-functionalized calix[4]arene derivatives interface energy barrier modified TiO_2 photoanode can enhance the injection and transport of electrons, and then retard the recombination of electrons, which results in a longer electron lifetime. The results shown here not only provide a new vision on how to produce highly efficient solar cells using modified TiO_2 photoanode with extended molecular structure but also open up a new way to position different photoanodes for interface modification.

Acknowledgment

“Authors would like to thank the European Union through the COST Action CM1202 “Supramolecular Photocatalytic Water Splitting (PERSPECT-H2O)” and the Scientific and Technological Research Council of Turkey (TUBITAK Grant Number 113T022) for the financial support of this research.”

Appendix A. Supplementary data

Supplementary data related to this article can be found at http://dx.doi.org/10.1016/j.jpowsour.2016.01.015.

References

[1] M.K. Nazeeruddin, A. Kay, I. Rodicio, R.H. Baker, E. Mueller, P. Liska, N. Vlachopoulos, M. Graetzel, J. Am. Chem. Soc. 115 (1993) 6382–6390.
[2] P. Wang, S.M. Zakeeruddin, J.E. Moser, M.K. Nazeeruddin, T. Sekiguchi, M. Gratzel, Nat. Mater 2 (2003) 402–407.
[3] G.A. Sewvandi, Z. Tao, T. Kusunose, Y. Tanaka, S. Nakanishi, Q. Feng, ACS Appl. Mater. Interfaces 6 (2014) 5818–5826.
[4] M.A. Beibei, G.A.O. Rui, W. Liduo, Z. Yifeng, S.H.I. Yantao, G. Yi, D. Haopeng, Q.I.U. Yong, Sci. China Chem. 53 (2010) 1669–1678.
[5] M.J. Katz, M.J.D. Vermeer, O.K. Farha, M.J. Pellin, J.T. Hupp, J. Phys. Chem. B 119 (2015) 7162–7169.
[6] J. Gong, J. Liang, K. Sumathy, Renew. Sust. Energy Rev. 16 (2012) 5848–5860.
[7] Y. Hua, Z. Shanqing, Z. Huijun, X.B. Fei, L. Porun, W. Geoffrey, J. Phys. Chem. C 113 (2009) 16277–16282.
[8] A. Kay, M. Gratzel, Chem. Mater 14 (2002) 2930–2935.
[9] G. Kumara, K. Tennakone, V.P.S. Perera, S. Kaneko, M. Okuya, J. Phys. D: Appl. Phys. 34 (2001) 868–873.
[10] E. Palomares, J.N. Clifford, S.A. Haque, T. Lutz, J.R. Durrant, J. Am. Chem. Soc. 125 (2003) 475–482.
[11] Y. Diamant, S. Chappel, S.G. Chen, O. Melamed, A. Zaban, Coord. Chem. Rev. 248 (2004) 1271–1276.
[12] Z. Xiang, X. Zhou, G. Wan, G. Zhang, D. Cao, ACS Sustain. Chem. Eng. 2 (2014) 1234–1240.
[13] M. Zukalova, A. Zukal, L. Kavan, M.K. Nazeeruddin, P. Liska, M. Graetzel, Nano Lett. 5 (2005) 1789–1792.
[14] H. Imahori, H. Yamada, Y. Nishimura, I. Yamazaki, Y. Sakata, J. Phys. Chem. B 104 (2000) 2099–2108.
[15] J. Holub, V. Eigner, L. Vrzal, H. Dvorakova, P. Lhotak, Chem. Commun. 49 (2013) 2798–2800.
[16] S. Sayin, E. Akoz, M. Yilmaz, Org. Biomol. Chem. 12 (2014) 6634–6642.
[17] P. Slavik, M. Dudic, K. Flidrova, J. Sykora, I. Cisarova, S. Bohm, P. Lhotak, Org. Lett. 14 (2012) 3628–3631.
[18] S. Sayin, M. Yilmaz, Tetrahedron 70 (2014) 6669–6676.
[19] A. Pandya, P.G. Sutariya, A. Lodha, S.K. Menon, Nanoscale 5 (2013) 2364–2371.
[20] D.O. Demirkol, H.B. Yildiz, S. Sayin, M. Yilmaz, RSC Adv. 4 (2014) 19900–19907.
[21] A. Acharya, K. Samanta, C.P. Rao, Coord. Chem. Rev. 256 (2012) 2096–2125.
[22] T. Laiho, J.A. Leiro, Appl. Surf. Sci. 252 (2006) 6304–6312.
[23] C.D. Gutsche, K.C. Nam, J. Am. Chem. Soc. 110 (1988) 6153–6162.
[24] Z.T. Li, G.Z. Ji, C.X. Zhao, S.D. Yuan, H. Ding, C. Huang, A.L. Du, M. Wei, J. Org. Chem. 64 (1999) 3572–3584.
[25] J.D.V. Loon, A. Arduini, L. Coppi, W. Verboom, A. Pochini, R. Ungaro, S. Harkema, D.N. Reinhoudt, J. Org. Chem. 55 (1990) 5639–5646.
[26] S. Bozkurt, M. Durmaz, M. Yilmaz, A. Sirit, Tetrahedron-Asymmetr 19 (2008) 618–623.
[27] S. Sönmezoğlu, C. Akyürek, S. Akın, J. Phys. D: Appl. Phys. 45 (2012) 425101–425106.
[28] S. Sönmezoğlu, C. Akyürek, H. Akış, IET Optoelectron 8 (2014) 270–276.
[29] S. Sayin, G.U. Akkuş, R. Cibulka, I. Stibor, M. Yilmaz, Helv. Chim. Acta 94 (2011) 481–486.
[30] S.P. Lim, A. Pandikumar, N.M. Huang, H.N. Lim, RSC Adv. 4 (2014) 38111–38118.
[31] Z. Sun, J.H. Kim, Y. Zhao, F. Bijarbooneh, V. Malgras, S.X. Dou, J. Mater. Chem. 22 (2012) 11711–11719.
[32] R. Hemmatzadeh, A. Mohammadi, J. Theor. Appl. Phys. 7 (2013) 57–63.
[33] M. Hilgendorff, V. Sundstrom, J. Phys. Chem. B 102 (1998) 10505–10514.
[34] X. Wu, J. Liu, Z. Chen, Q. Yang, C. Li, G. Lu, L. Wang, J. Mater. Chem. 22 (2012) 10438–10440.
[35] S.E. Koops, B.C. O'Regan, P.R.F. Barnes, J.R. Durrant, J. Am. Chem. Soc. 131 (2009) 4808–4818.
[36] G. Dai, L. Zhao, S. Wang, J. Hu, B. Dong, H. Lu, J. Li, J. Alloy Compd. 539 (2012) 264–270.
[37] R.G. Compton, J. Wadhawan, Electrochemistry: Nanoelectrochemistry, Royal Society of Chemistry, 2013.
[38] R. Bhattacharjeez, I.M. Hung, ECS Solid State Lett. 2 (2013) Q101–Q104.
[39] S. Ferrere, B.A. Gregg, J. Am. Chem. Soc. 120 (1998) 843–844.
[40] U. Rammelt, G. Reinhard, Electrochem. Acta 35 (1990) 1045–1049.
[41] C.H. Hsu, F. Mansfeld, Corrosion 57 (2001) 747–748.
[42] C.P. Hsua, K.M. Lee, J.T.W. Huangb, C.Y. Linb, C.H. Lee, L.P. Wang, S.Y. Tsaic, K.C. Ho, Electrochim. Acta (2008) 7514–7522.